ANOMALOUS DIFFUSION IN BIOMOLECULAR SYSTEMS FROM THE PERSPECTIVE OF NON-EQUILIBRIUM STATISTICAL PHYSICS

Gerald Kneller

Centre de Biophysique Moléculaire CNRS
Rue Charles Sadron, 45071 Orléans, France
and
Synchrotron SOLEIL, Saint Aubin — BP 48, 91192 Gif-sur-Yvette, France
and
Université d'Orléans, Avenue du Parc Floral, 45067 Orléans, France

(Received March 18, 2015)

This contribution gives a short introduction into the theory of anomalous diffusion and relaxation with illustrations from computer simulations of biomolecular systems. The theory is presented from the perspective of the non-equilibrium statistical physics, confronting stochastic models with exact results which have been recently obtained on the basis of asymptotic analysis. In this context, conditions for anomalous diffusion will be discussed and the Kubo relations for the fractional diffusion and relaxation constant will be derived.

DOI:10.5506/APhysPolB.46.1167
PACS numbers: 05.10.Gg, 05.40.Jc, 05.40.Fb

1. Introduction

Anomalous diffusion is a vast and exciting topic, in particular for "crowded" biological systems, where the transport of molecules plays a central functional role. In this context, many findings have been made over the last 20 years, in particular with the advent of new spectroscopic techniques. There is a vast amount of papers on the subject, including papers on the theoretical description of anomalous diffusion. The reader is here referred to the seminal paper on fractional Brownian motion by Mandelbrot and Van Ness [1], the paper by Scher and Montroll on the Continuous Time Random Walk [2] and the review articles by Metzler [3] and Sokolov [4]. The idea of this paper is to look at the anomalous diffusion from the perspective of non-equilibrium statistical physics, referring in this context to concepts such as the Generalized Langevin Equation (GLE) [5, 6] and Kubo relations

for transport coefficients [7]. For this purpose, several recent papers on that topic are presented in a concise way, starting with classical diffusion models and their mathematical extensions for the description of anomalous diffusion and relaxation. These models are then related to exact results, which are obtained by asymptotic analysis of the GLE and the related mean square displacements, and the latter are illustrated by molecular dynamics simulations of biomolecular systems.

2. Some models for anomalous diffusion

2.1. Generalized diffusion equation

The first theoretical description of diffusion processes can probably be attributed to the physician and physiologist Fick [8]. He derived the well-known diffusion equation,

$$\frac{\partial}{\partial t} f(\boldsymbol{r}, t) = D \Delta f(\boldsymbol{r}, t)\,, \tag{1}$$

to model the time evolution of concentration profiles of particles in suspension. Here, D is the diffusion coefficient, which is a transport coefficient in the language of statistical physics. The diffusion equation holds in the regime of linear response, where the particle current density responds linearly to the concentration gradient, $\boldsymbol{j} = -D\boldsymbol{\nabla} f$ (first law of Fick). Imposing particle conservation through $\partial_t f + \boldsymbol{\nabla} \cdot \boldsymbol{j} = 0$ (second law of Fick), Eq. (1) follows. In this description, one considers free diffusion, *i.e.* diffusion without a systematic driving force. The diffusion constant D determines the spread of the concentration,

$$\sigma^2(t) := \frac{\int d^n r\, |\boldsymbol{r}|^2 f(\boldsymbol{r}, t)}{\int d^n r\, f(\boldsymbol{r}, t)} = 2nDt\,, \tag{2}$$

assuming that the initial concentration is localized at $\boldsymbol{r} = \boldsymbol{0}$. Here, n is the geometrical dimension of the diffusion problem and we assume isotropic diffusion, such that the total spread is the sum of n independent identical contributions $2Dt$.

Deviations from the diffusion law (2) have been reported already 80 years ago [9] and with the advent of sophisticated fluorescence-based spectroscopic methods, numerous observations of anomalous diffusion have been reported over the last 20 years. Typical examples are the diffusion of molecules in biological membranes and lipid model bilayers [10–12], where the diffusion of lipid molecules and embedded proteins is strongly hindered due to the entanglement with their environment. The effect is often referred to as crowding and leads to *subdiffusion*, where

$$\sigma^2(t) \propto t^{\alpha} \tag{3}$$

with $0 < \alpha < 1$. Concentration profiles with an "anomalous" spread of the form (3) can be obtained by an appropriate generalization of the diffusion equation (1) in form of a fractional diffusion equation [3, 13]

$$\frac{\partial}{\partial t} f(\boldsymbol{r}, t) = \partial_t^{1-\alpha} \left\{ D_\alpha \Delta f(\boldsymbol{r}, t) \right\} , \qquad 0 < \alpha < 2 , \tag{4}$$

where D_α is a fractional diffusion constant and $\partial_t^{1-\alpha}$ denotes a fractional Riemann–Liouville derivative of the order of $1 - \alpha$ with respect to time [14, 15]. For an arbitrary function $g(t)$, the latter is defined as

$$\partial_t^{1-\alpha} g(t) = \frac{d}{dt} \int_0^t d\tau \, \frac{(t-\tau)^{\alpha-1}}{\Gamma(\alpha)} g(\tau) , \tag{5}$$

where $\Gamma(.)$ denotes the Gamma function or generalized factorial [16]. For $\alpha = 1, 2, 3, \ldots$, the integral $\int_0^t \ldots$ becomes the familiar Liouville formula for a multiple integration of g. One may effectively write $\partial_t^{1-\alpha} g(t) = d/dt \, I_t^\alpha g(t)$, where $I_t^\alpha g(t)$ denotes a fractional integration of the order of α. The time evolution of the spread can be computed from the fractional differential equation,

$$\partial_t \sigma^2(t) = \partial_t^{1-\alpha} 2nD_\alpha , \tag{6}$$

which follows from the definition of σ and from (4), and which can be solved straightforwardly by Laplace transform to yield

$$\sigma^2(t) = \frac{2nD_\alpha t^\alpha}{\Gamma(1+\alpha)} . \tag{7}$$

In view of relation (3), this is the desired result.

2.2. Fractional Fokker–Planck equations for spatial diffusion

Instead of modeling diffusion as a macroscopic migration process, one can take the perspective of individual particles as representatives for the whole ensemble and develop models for their trajectories. This route has been proposed in the pioneering work of Einstein and Smoluchowski [17–20] and lead to the theory of stochastic processes [21–23]. In this approach, the concentration profile becomes a conditional probability $p(\boldsymbol{r}, t|\boldsymbol{r}_0, 0)$ for a transition $\boldsymbol{r}_0 \to \boldsymbol{r}$ within time t, and instead of the concentration spread one considers the mean square displacement (MSD) of the diffusing particles,

$$\begin{aligned} W(t) &= \left\langle |\boldsymbol{r}(t) - \boldsymbol{r}(0)|^2 \right\rangle \\ &\equiv \int\int d^n r_0 d^n r \, |\boldsymbol{r} - \boldsymbol{r}_0|^2 p(\boldsymbol{r}, t|\boldsymbol{r}_0, 0) p_{\mathrm{eq}}(\boldsymbol{r}_0) , \end{aligned} \tag{8}$$

where $p_{\mathrm{eq}}(\boldsymbol{r}_0)$ is the equilibrium distribution. Using molecular trajectories from experiments, such as Single Particle Tracking (SPT) of fluorescently labeled molecules [24–26] and molecular dynamics simulations [27, 28], MSDs may be approximated by ($t > 0$)

$$W(t) \approx \frac{1}{T-t} \int_0^{T-t} d\tau \, |\boldsymbol{r}(\tau + t) - \boldsymbol{r}(\tau)|^2 \,, \tag{9}$$

where T is the trajectory length.

In the case of normal diffusion, the time evolution of the transition probabilities is described by Fokker–Planck equations (FPEs) [29], which are derived by assuming that the underlying stochastic process is Markovian and that small-step diffusion processes are considered. In order to include anomalous diffusion, these FPEs can be generalized to corresponding fractional counterparts, fractional Fokker–Planck equations (fFPEs), applying the same "recipe" as for the fractional diffusion equation (4),

$$\frac{\partial}{\partial t} p(\boldsymbol{r}, t|\boldsymbol{r}_0, 0) = \partial_t^{1-\rho} \, \mathcal{L} p(\boldsymbol{r}, t|\boldsymbol{r}_0, 0) \,, \tag{10}$$

where ρ depends on the context. The Fokker–Planck operator $\mathcal{L}$ has, in general, the Smoluchowski form [30],

$$\mathcal{L} = D_\rho \frac{\partial}{\partial \boldsymbol{r}} \cdot \left\{ \frac{\partial}{\partial \boldsymbol{r}} + \frac{1}{k_{\mathrm{B}} T} \frac{\partial V(\boldsymbol{r})}{\partial \boldsymbol{r}} \right\} , \tag{11}$$

where $V(\boldsymbol{r})$ is an external potential and the parameter D_ρ is a fractional diffusion constant. The fFPE (10) is to be solved with the initial condition $p(\boldsymbol{r}, 0|\boldsymbol{r}_0, 0) = \delta(\boldsymbol{r} - \boldsymbol{r}_0)$ and for long times the resulting solution tends to the equilibrium probability density, $p_{\mathrm{eq}}(\boldsymbol{r}) = \lim_{t\to\infty} p(\boldsymbol{r}, t|\boldsymbol{r}_0, 0)$. Two cases must be distinguished.

1. Free anomalous diffusion. Here, $V = 0$ and the MSD behaves asymptotically as $W(t) \sim t^\alpha$, with $0 \leq \alpha < 2$, and $\rho \equiv \alpha$.

2. Confined anomalous diffusion. Here, $V \neq 0$ leads to a confinement, such that asymptotically $W(t) \sim$ const and therefore $\alpha = 0$. In this case, $\rho \equiv \beta$ and $0 < \beta \leq 1$ describes how the MSD converges to its plateau value. The parameters α and β are thus intrinsically different and we come back to this point in Section 3.4.

Similarly to the diffusion equation, the fFPE (10) can be written in the form of an equation of continuity, $\partial_t f + \boldsymbol{\nabla} \cdot \boldsymbol{j} = 0$, which expresses here the conservation of probability and where $\boldsymbol{j}$ has the form

$$\boldsymbol{j}(\boldsymbol{r}, t) = -D_\rho \partial_t^{1-\rho} \left\{ \frac{\partial f(\boldsymbol{r}, t)}{\partial \boldsymbol{r}} + \frac{1}{k_\mathrm{B} T} \frac{\partial V(\boldsymbol{r})}{\partial \boldsymbol{r}} \right\} . \tag{12}$$

Compared to Fick's first law, there are two generalizations to be mentioned. Firstly, there is a drift term due to the external potential, and secondly, it follows from Eq. (5) that the fractional derivative induces *memory effects* in the response of $\boldsymbol{j}$ to the concentration gradient and the potential gradient. It must be emphasized that the above phenomenological interpretation of anomalous diffusion is not the only route to anomalous diffusion and fFPEs, but it is conceptually close to the framework of non-equilibrium statistical physics which will be used in the following discussion.

2.3. Fractional Wiener process

In the case of free diffusion, *i.e.* for $V(\boldsymbol{r}) = 0$, $p(\boldsymbol{r}, t|\boldsymbol{r}_0, 0)$ describes a Wiener process, which is generalized to a fractional variant if anomalous diffusion is considered. The corresponding fFPE reads

$$\frac{\partial}{\partial t} p(\boldsymbol{r}, t|\boldsymbol{r}_0, 0) = \partial_t^{1-\alpha} D_\alpha \Delta p(\boldsymbol{r}, t|\boldsymbol{r}_0, 0) , \qquad 0 < \alpha < 2 \tag{13}$$

and the MSD can be easily computed by using that the equilibrium distribution is here $p_\mathrm{eq}(\boldsymbol{r}) = 1/V$, where V is the macroscopic volume ($V \to \infty$) in which the diffusion process takes place

$$W(t) = \frac{2nD_\alpha t^\alpha}{\Gamma(1+\alpha)} . \tag{14}$$

The MSD has thus exactly the same form as the particle spread for the generalized Fick model (see Eq. (7)). It should be noted that (13) does not only include the subdiffusive regime mentioned earlier, where $0 < \alpha < 1$, but also a *superdiffusive*, sub-ballistic regime, where $1 < \alpha < 2$. The latter has, for example, been found in experiments on chemotaxis [31].

2.4. Fractional Ornstein–Uhlenbeck process

2.4.1. Confined motions — diffusion and relaxation

We consider now a diffusing particle whose motions are confined in space. Due to the confinement, it has a well-defined mean position and introducing $\boldsymbol{u}(t) = \boldsymbol{r}(t) - \langle \boldsymbol{r} \rangle$, it follows that

$$W(t) = 2\{c_{uu}(0) - c_{uu}(t)\} , \tag{15}$$

where

$$c_{uu}(t) = \langle \boldsymbol{u}(t) \cdot \boldsymbol{u}(0) \rangle \tag{16}$$

is the displacement autocorrelation function (DACF) of the diffusing particle. Relation (15) reflects thus at the same time diffusion and relaxation in position space. Knowing that $\lim_{t\to\infty} c_{uu}(t) = 0$ and that $c_{uu}(0) = \langle |\boldsymbol{u}|^2 \rangle$ is the mean square position fluctuation, it follows from (15) that

$$\lim_{t\to\infty} W(t) = 2 \left\langle |\boldsymbol{u}|^2 \right\rangle . \tag{17}$$

2.4.2. The model

A simple example for a concrete dynamical model is the fractional Ornstein–Uhlenbeck (fOU) process [3, 32, 33] which describes anomalous diffusion of a Brownian particle in a harmonic potential,

$$V(\boldsymbol{u}) = \frac{K}{2} |\boldsymbol{u}|^2 , \qquad K > 0 . \tag{18}$$

The corresponding transition probability density is described by the fFPE

$$\frac{\partial}{\partial t} p(\boldsymbol{u}, t|\boldsymbol{u}_0, 0) = \partial_t^{1-\beta} \mathcal{L}\, p(\boldsymbol{u}, t|\boldsymbol{u}_0, 0) , \qquad 0 < \beta \leq 1 , \tag{19}$$

where the Fokker–Planck operator reads

$$\mathcal{L} = D_\beta \frac{\partial}{\partial \boldsymbol{u}} \cdot \left\{ \frac{\partial}{\partial \boldsymbol{u}} + \frac{K\boldsymbol{u}}{k_\mathrm{B}T} \right\} . \tag{20}$$

Here k_B and T denote, respectively, the Boltzmann constant and the absolute temperature. Due to the Hookean force, $F(\boldsymbol{u}) = -K\boldsymbol{u}$, the equilibrium probability density tends for long times to a Gaussian function of finite width,

$$p_\mathrm{eq}(\boldsymbol{u}) = \sqrt{\frac{K}{2\pi k_\mathrm{B}T}}^{\,n} \exp\left(-\frac{K|\boldsymbol{u}|^2}{2k_\mathrm{B}T} \right) . \tag{21}$$

With these definitions, the DACF for the fOU process is obtained via

$$c_{uu}(t) \equiv \int_{-\infty}^{\infty} \int_{-\infty}^{\infty} d^n u_0 d^n u\, \boldsymbol{u} \cdot \boldsymbol{u}_0\, p(\boldsymbol{u}, t|\boldsymbol{u}_0, 0) p_\mathrm{eq}(\boldsymbol{u}_0) , \tag{22}$$

but the full solution $p(\boldsymbol{u}, t|\boldsymbol{u}_0, 0)$ is not required for its computation. One can, in fact, apply a similar trick as for the MSD of anomalous free diffusion

and establish a fractional differential equation for $c_{uu}(t)$, whose solution is found to be [33]

$$c_{uu}(t) = \left\langle |\boldsymbol{u}|^2 \right\rangle E_\beta \left(-[t/\tau]^\beta \right) . \tag{23}$$

Here, the mean square position fluctuation is given by

$$\left\langle |\boldsymbol{u}|^2 \right\rangle = n k_\mathrm{B} T / K , \tag{24}$$

$E_\beta(z)$ denotes the Mittag–Leffler function [16], and the time scale τ is defined by the relation

$$\tau = \left(\frac{n D_\beta}{\left\langle |\boldsymbol{u}|^2 \right\rangle} \right)^{-1/\beta} . \tag{25}$$

The Mittag–Leffler function is an entire function in the complex plane,

$$E_\beta(z) = \sum_{k=0}^{\infty} \frac{z^k}{\Gamma(1+\beta k)} , \tag{26}$$

and can be considered as a generalization of a normal exponential function. For $\beta = 1$, the latter is retrieved, $E_1(z) = \exp(z)$. According to (15), the MSD takes the form

$$W(t) = 2 \left\langle |\boldsymbol{u}|^2 \right\rangle \left(1 - E_\beta \left(-[t/\tau]^\beta \right) \right) \tag{27}$$

and two regimes can be distinguished:

(a) The *short time regime*, where $t \ll \tau$. Here, one may use just the first two terms of the series (26), such that

$$W(t) \overset{t \ll \tau}{\sim} \frac{2 n D_\beta}{\Gamma(1+\beta)} t^\beta . \tag{28}$$

(b) The *long time regime*, where $t \gg \tau$. Here, it follows from

$$E_\beta \left(-[t/\tau]^\beta \right) \overset{t \gg \tau}{\sim} \frac{(t/\tau)^{-\beta}}{\Gamma(1-\beta)} \tag{29}$$

that the MSD behaves as

$$W(t) \overset{t \gg \tau}{\sim} 2 \left\langle |\boldsymbol{u}|^2 \right\rangle \left(1 - \frac{(t/\tau)^{-\beta}}{\Gamma(1-\beta)} \right) . \tag{30}$$

Since $\lim_{\beta \to 1} \Gamma(1-\beta) = +\infty$, the long-time tail vanishes for normal diffusion. Here, the Mittag–Leffler function becomes a normal exponential function, $E_1(z) = \exp(z)$, and one retrieves the exponentially relaxing DACF of the normal Ornstein–Uhlenbeck process.

2.4.3. Relaxation rate spectrum

It is illustrative to express the DACF (23) as a continuous superposition of exponential functions [33, 34], which reflects the multiscale character of the relaxation dynamics described by the fOU process. Defining the normalized autocorrelation function (relaxation function)

$$\psi(t) = c_{uu}(t)/c_{uu}(0)\,, \tag{31}$$

one writes then

$$\psi(t) = \int_0^\infty d\lambda\, p(\lambda) \exp(-\lambda t), \tag{32}$$

where $p(\lambda)$ must be positive and must also satisfy the normalization condition $\int_0^\infty d\lambda\, p(\lambda) = 1$. The relaxation rate spectrum is intimately related to the Laplace transform of the DACF, which can be written as a Stieltjes transform [16] of $p(\lambda)$

$$\hat{\psi}(s) = \int_0^\infty d\lambda\, \frac{p(\lambda)}{s+\lambda}\,, \tag{33}$$

$$p(\lambda) = \frac{1}{\pi} \lim_{\epsilon\to 0} \Im\left\{\hat{\psi}(-\lambda - i\epsilon)\right\}\,. \tag{34}$$

On a dimensionless time scale, the relaxation function has the form

$$\psi_{\mathrm{fOU}}(t;\beta) = E_\beta\left(-t^\beta\right) \tag{35}$$

and from its Laplace transform [35]

$$\hat{\psi}_{\mathrm{fOU}}(s;\beta) = \frac{1}{s\left(1+s^{-\beta}\right)}\,, \tag{36}$$

one finds the corresponding relaxation rate spectrum

$$p_{\mathrm{fOU}}(\lambda;\beta) = \frac{\sin(\pi\beta)}{\lambda\left(\lambda^{-\beta}+\lambda^{\beta}+2\cos(\pi\beta)\right)}\,. \tag{37}$$

Exponential relaxation is obtained for $\beta \to 1$, *i.e.*

$$\lim_{\beta\to 1} p_{\mathrm{fOU}}(\lambda;\beta) = \delta(\lambda-1)\,. \tag{38}$$

The relaxation function $\psi(t;\beta)$ and the corresponding relaxation rate spectrum for some values of β are shown in Fig. 1. One observes that $p_{\mathrm{fOU}}(\lambda;\beta)$ develops a peak around $\lambda = 1$ as β approaches one.

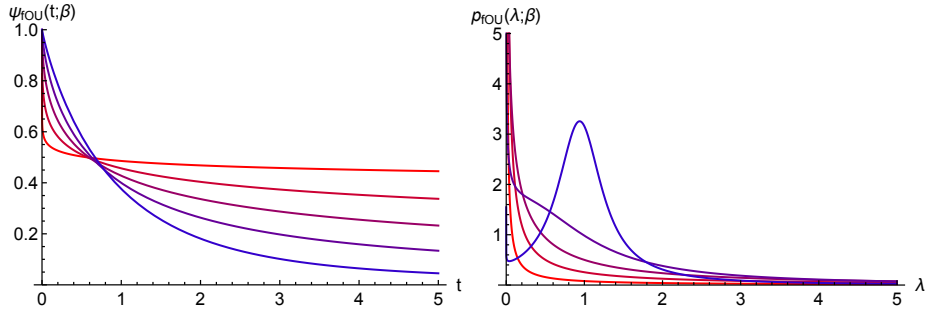

Fig. 1. Left: Normalized DACF $\psi_{\mathrm{fOU}}(t;\beta)$ for $\beta = 0.1, 0.3, \ldots, 0.9$ (curves from top to bottom/red to blue on-line). Right: Corresponding relaxation spectra $p_{\mathrm{fOU}}(\lambda;\beta)$.

2.5. Anomalous Brownian motion in velocity space

Diffusion may be as well described by stochastic processes in velocity space. In this case, one considers a conditional probability density $p(\boldsymbol{v}, t|\boldsymbol{v}_0, 0)$ for a velocity change $\boldsymbol{v}_0 \to \boldsymbol{v}$ within time t. The process must be constructed such that $p(\boldsymbol{v}, t|\boldsymbol{v}_0, 0)$ tends towards a Maxwell distribution for long times, independently if the process is normal or anomalous. In the case of normal diffusion, one considers an Ornstein–Uhlenbeck process in velocity space and the diffusing particle is referred to as a Rayleigh particle [23]. To account for anomalous diffusion, Barkay and Silbey [36] proposed a corresponding fFPE of the form

$$\frac{\partial}{\partial t} p(\boldsymbol{v}, t|\boldsymbol{v}_0, 0) = \partial_t^{1-\rho} \mathcal{L}_v \, p(\boldsymbol{v}, t|\boldsymbol{v}_0, 0) \,, \qquad 0 < \rho < 2 \,, \tag{39}$$

where the Fokker–Planck operator $\mathcal{L}_v$ has the form

$$\mathcal{L}_v = \eta_\rho \left\{ \frac{\partial}{\partial \boldsymbol{v}} \cdot \boldsymbol{v} + \frac{k_{\mathrm{B}} T}{m} \frac{\partial}{\partial \boldsymbol{v}} \cdot \frac{\partial}{\partial \boldsymbol{v}} \right\} . \tag{40}$$

The parameter η_ρ is a fractional relaxation constant with dimension $1/\mathrm{s}^\rho$ in SI units. Here, the equilibrium solution of (39) is indeed the Maxwell distribution, and, analogously to (23), one finds that the velocity autocorrelation function (VACF) has the form

$$c_{vv}(t) = \left\langle |\boldsymbol{v}|^2 \right\rangle E_\rho \left(-[t/\tau_v]^\rho \right) . \tag{41}$$

The time scale τ_v is defined through

$$\tau_v = (1/\eta_\rho)^{1/\rho} \tag{42}$$

and $\langle|\boldsymbol{v}|^2\rangle = nk_{\mathrm{B}}T/M$. In order to construct the MSD from the VACF of a diffusing particle, one expresses displacements as integrals over velocities, such that $W(t) = \langle\int_0^t \int_0^t d\tau_1 d\tau_2\, \boldsymbol{v}(\tau_1)\cdot\boldsymbol{v}(\tau_2)\rangle$. Assuming stationarity of the underlying process and a classical dynamical system, this may be expressed in the form

$$W(t) = 2\int_0^\infty d\tau\,(t-\tau)c_{vv}(\tau)\,. \tag{43}$$

Two regimes can again be distinguished:

(a) The *short time regime*, where $t \ll \tau_v$. This is the so-called "ballistic regime" which corresponds to free flight, where $c_{vv}(t) \approx \langle|\boldsymbol{v}|^2\rangle$, such that

$$W(t) \overset{t\ll\tau_v}{\sim} \langle|\boldsymbol{v}|^2\rangle\, t^2\,. \tag{44}$$

(b) The *long time regime*, where $t \gg \tau_v$. Using the Laplace transform of $W(t)$, relation (43) becomes $\hat{W}(s) = 2\hat{c}_{vv}(s)/s^2$, where one may use that (see Eq. (36))

$$\hat{c}_{vv}(s) = \frac{\langle|\boldsymbol{v}|^2\rangle}{s(1+(s\tau_v)^{-\rho})}\,. \tag{45}$$

The asymptotic form of the MSD reads therefore

$$W(t) \overset{t\gg\tau_v}{\sim} \frac{2\langle|\boldsymbol{v}|^2\rangle\,\tau_v^\rho}{\Gamma(3-\rho)}t^{2-\rho}\,. \tag{46}$$

Setting

$$\rho = 2-\alpha \qquad \text{with} \qquad 0<\alpha<2\,, \tag{47}$$

the MSD takes the form (14), where

$$D_\alpha = \frac{\langle|\boldsymbol{v}|^2\rangle}{n}\eta_{2-\alpha}^{-1} \tag{48}$$

is the fractional diffusion coefficient.

2.6. Illustrations

In this section, two examples are presented for anomalous diffusion and relaxation in biomolecular systems seen by molecular dynamics simulations.

2.6.1. Lateral diffusion in lipid bilayers

As mentioned earlier, there is an experimental evidence by fluorescence-based techniques that the lateral diffusion of molecules in lipid bilayers is anomalous [10–12], and several groups have recently studied these motions by molecular dynamics simulations [37–39]. It must be emphasized that the experimental data concern much longer time scales (micro- to milliseconds) than those accessible by MD simulations, which are roughly limited to 100 nanoseconds for all-atom models and today's standard computer equipment. The interesting question is now if the experimentally found subdiffusion is also seen on the much shorter time scales of MD simulations and if the fractional diffusion constants are comparable.

The left part of Fig. 2 displays the MSD of a simulated lipid bilayer consisting of 128 (2×64) dioleoyl-sn-glycero-3-phosphocholine (DOPC) molecules, which are hydrated by 3840 water molecules in total. The right part of the figure shows the simulated system, where the water molecules are indicated in light gray and the tails of the lipid molecules in dark gray/green. For details of the simulation, the reader is referred to Ref. [37] and here it is only mentioned that the length of the MD production run was 160 nanoseconds. This is thus approximately 5 times longer than the MSD lag time in Fig. 2. Statistical accuracy is an important issue in the estimation of MSDs through Eq. (9) and the main problem is here that inaccuracies sneak in

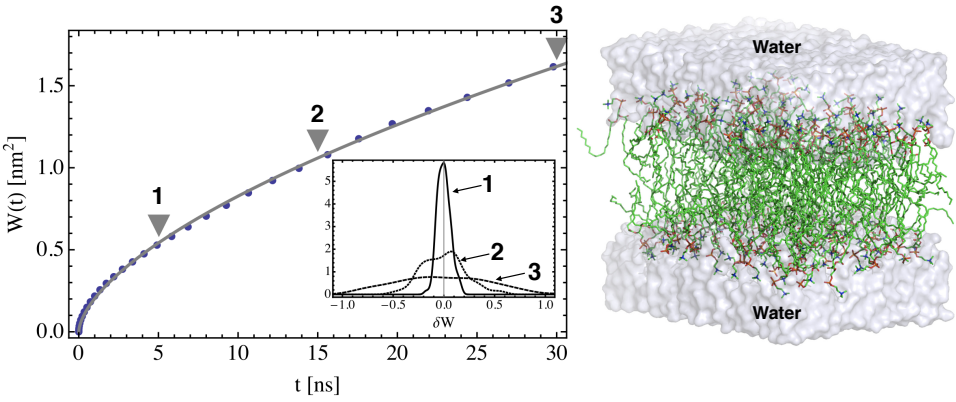

Fig. 2. Left: Simulated molecule-averaged MSD for the lateral center-of-mass diffusion of the DOPC molecules (dots) and fit of model (14), with $n = 2$ (solid line, see the text). The fitted fractional diffusion coefficient is $D_\alpha = 0.045$ nm^2/ns$^\alpha$ for $\alpha = 0.61$. The inset shows the spread of the individual molecular MSDs with respect to the molecule averaged MSD at $t = 5$ ns (label 1), at $t = 15$ ns (label 2), and at $t = 30$ ns (label 3). In the main figure, the corresponding average MSD values are indicated by correspondingly labeled triangles [37]. Right: Simulated system consisting of a bilayer of 2×64 DOPC lipid molecules and 3840 water molecules (light gray) [37].

gradually with increasing lag time. As a rule of thumb, the latter should be roughly an order of magnitude smaller than the length of the simulated trajectory.

Since all lipid molecules are physically equivalent, their MSDs can be averaged to estimate the fractional diffusion constant. This increases the statistical accuracy considerably and the effect can be seen in the inset of the left part of Fig. 2, which displays the spread of the individual MSDs. If D_α is here defined according to relation (14), with $n = 2$, one finds $D_\alpha = 0.045$ nm^2/ns$^\alpha$. It should be noted that in [37] the definition $W(t) = 2D_\alpha t^\alpha$ has been used for the asymptotic form of the MSD, which leads to $D_\alpha = 0.101$ nm^2/ns$^\alpha$. What matters is that the experimental value for DLPC (dilauroyl-sn-glycero-3-phosphocholine) in Ref. [10] is approximately $D_\alpha = 0.02$ nm^2/ns$^\alpha$ and thus clearly of the same order of magnitude. This is an interesting result since fluorescence correlation spectroscopy explores the millisecond to second time scale, which is about 7 orders of magnitude larger than time scale of MD simulations.

The accessible time scale to simulations can be extended by using coarse-grained models, in which several atoms are grouped into one "pseudo-atom", and such simulations for fully hydrated POPC (1-palmitoyl-2-oleoyl-sn-glycero-3-phosphocholine) bilayers have been recently performed [40], comparing the results obtained from MD simulations with the all-atom OPLS force field [41, 42] and the coarse-grained MARTINI force field [43, 44]. All simulation details can be found in Ref. [40] and here only the most important parameters are reported. The all-atom system comprises a bilayer of 274 POPC lipids immersed in 10 471 water molecules and the coarse-grained system 2033 POPC molecules immersed in 231 808 water molecules (see Fig. 3). The corresponding simulation lengths were 15 nanoseconds in the case of

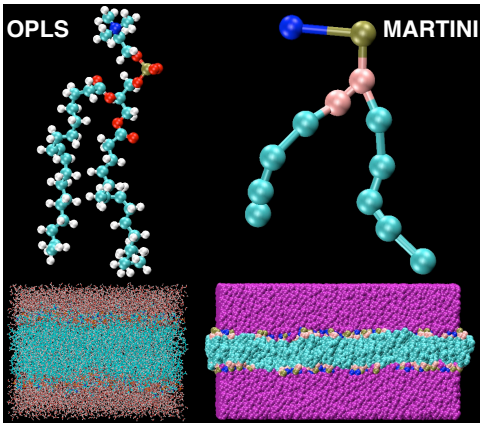

Fig. 3. Simulated all-atom (OPLS f.f.) and coarse-grained (MARTINI f.f.) systems for a POPC bilayer.

the all-atom system and 600 nanoseconds for the coarse-grained system. In the latter case, simulations were performed in the NVT-ensemble, *i.e.* at constant volume and temperature, and in the so-called "NAp$_z$T-ensemble", where the membrane surface is constant but the volume can slightly change perpendicular to the membrane [44]. The idea in the latter case is to maintain the surface per lipid molecule strictly. All relevant parameters are reported in Table I and show that lateral subdiffusion is observed for both the all-atom and the coarse-grained system, but the diffusion coefficient for the coarse-grained system is about three times bigger. Comparing the fractional diffusion coefficient to the one of DOPC (see inset of Fig. 2) shows also that POPC diffuses more slowly than DOPC, noting that the exponents α have similar values.

TABLE I

Coefficient α and fractional diffusion coefficient D_α for the OPLS all-atom (AA) simulation of POPC and the coarse-grained (CG) MARTINI force field [40]. Here "short" refers to the left part of Fig. 4 (time lag 1.5 ns) and "long" to the right part (time lag 50 ns). The fractional diffusion constant is defined according to relation (14) and (1) and (2) refer, respectively, to the simulation with the NAp$_z$T- and NVT-ensemble.

	AA short	CG(1) short	CG(2) short	CG(1) long	CG(2) long
α	0.668	0.515	0.508	0.571	0.558
D_α [nm^2/ns$^\alpha$]	0.0081	0.026	0.026	0.023	0.023

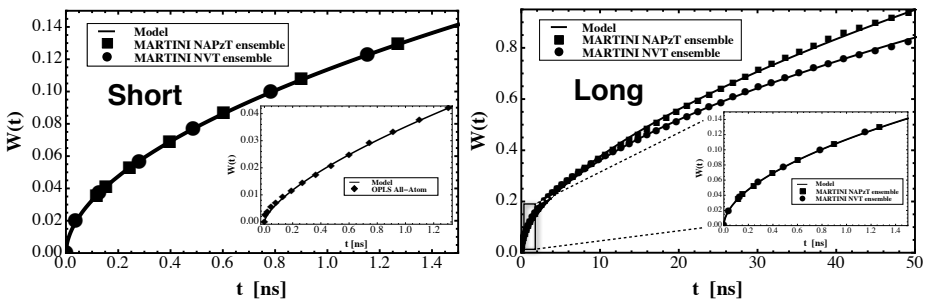

Fig. 4. Left: Molecule-averaged MSD for the lateral center-of-mass diffusion of POPC molecules from the coarse-grained model, where circles refer to the NPT-ensemble and square to the sNAp$_z$T-ensemble, and the fit of model (14) (solid line). The inset displays the MSD for the all-atom model on the same time scale (circles) together with the fit of model (14) (solid line). Right: Molecule averaged lateral MSDs for POPC from the coars-grained model on a longer time scale. The legend is the same as in the left part of the figure. The inset shows that the MSDs for the NVT-ensemble and the NAp$_z$T-ensemble cannot be distinguished on short time scales.

2.6.2. Diffusive atomic motions in proteins

The following example shows that the fractional Ornstein–Uhlenbeck process is a good model for protein dynamics on the atomic level. It is, in fact, probably the simplest model being able to account for the following two facts:

1. Atomic motions in proteins are confined in space if global translations and rotations of the whole protein are subtracted.
2. The spectrum of associated time scales is vast, ranging from femtoseconds to hours.

Experimental information about motional amplitudes has first been obtained from protein crystallography [45, 46] and from thermal neutron scattering [47, 48]. Early studies of protein reaction kinetics by laser flash photolysis of CO in myoglobin [49] gave already evidence for the multiscale character of internal diffusion and relaxation processes and lead to the concept of complex, "rugged" potential energy landscapes of proteins which contains a large number of local minima — also referred to as conformational substates [50] — and whose envelope defines an effective potential. The motion in this effective potential can be modeled as a diffusion process describing the multiple irregular transitions between the substates which are not resolved in time. In this picture, the strongly non-exponential binding kinetics observed by flash photolysis experiments is caused by a broad distribution of barrier heights separating the substates [34]. A sketch of a "rugged" potential energy landscape with a parabolic envelope is depicted in Fig. 5.

The multiscale character of protein dynamics has also been emphasized by more recent fluorescence correlation studies of distance fluctuations in flavin reductase between flavin as a fluorescent site and a nearby tyrosine acting as a quenching site [51]. The interesting point is that such experiments can be performed on single molecules. On the theoretical side, they have been interpreted with a generalized Fokker–Planck equation containing a power-law memory kernel, which leads to a distance autocorrelation function in form of "stretched" Mittag–Leffler function [52], which is also the form of the position autocorrelation for the fractional Ornstein–Uhlenbeck process (*cf.* Eq. (23)). This was the motivation in Ref. [33] to introduce the fOU process as a model for the dynamics of atoms in proteins probed by Molecular Dynamics simulations and neutron scattering. The model is, in fact, an extension of the harmonic oscillator model which is widely used for the interpretation of the elastic incoherent neutron scattering factor of proteins [48]. In contrast to the latter, it does not only model the motional amplitudes but also the diffusive multiscale dynamics of atoms in proteins. An application can be found in the combined neutron scattering and simulation study [53],

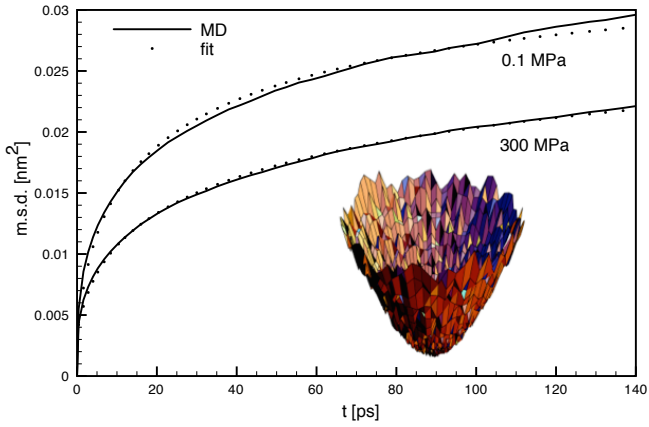

Fig. 5. Average atomic mean-square displacement of lysozyme in solution from MD simulation (solid lines) [53]. Here $W(t) = \langle (x(t) - x(0))^2 \rangle$, where x stands for the displacement in an arbitrary direction. The upper curve corresponds to normal pressure ($p = 0.1$ MPa) and the lower curve to a pressure of $p = 300$ MPa. More explanations are given in the text. The inset shows a sketch of a "rugged" potential energy surface for the fOU process. More explanations are given in the text.

where the model is used to quantify the influence of a non-denaturing hydrostatic pressure (3 kbar) on lysozyme. Figure 5 shows the average time-dependent MSD for the atoms in lysozyme (solid lines) and the fits of the corresponding model (27) (dotted lines). The inset displays a sketch for the "rugged" potential energy surface of a two-dimensional fOU process. Not surprisingly, the application of pressure leads to a reduction of the motional amplitudes, which are found to be $\langle x^2 \rangle = 6.17 \times 10^{-3}$ nm^2 at normal pressure and $\langle x^2 \rangle = 4.74 \times 10^{-3}$ nm^2 at 3 kbar. The MSD is here considered for the displacement in an arbitrary direction, $W(t) = \langle (x(t) - x(0))^2 \rangle$ and $\langle x^2 \rangle = \langle |\boldsymbol{u}|^2 \rangle / 3$, assuming isotropic motions. More interesting is that the β-parameter stays unchanged under pressure, namely $\beta \approx 0.5$, whereas the fitted values for τ indicate the motions become slower: $\tau = 31.75$ ps for normal pressure and $\tau = 39.08$ ps for 3 kbar. This means that pressure makes the dynamics slower but leaves its characteristics unchanged. The value of $\beta \approx 0.5$ indicates that the diffusion is far from normal and the form of the corresponding relaxation rate spectrum can be read off from Fig. 1.

It is finally worthwhile mentioning that the fOU model has also been successfully used to model experimental data from NMR relaxation spectroscopy, where it accounts for the strongly non-exponential decay of reorientational correlation function of $(N - H)$ bond vectors [54–57]. Formally, one replaces here the exponential function in the widely used "model-free" interpretation of experimental relaxation times [58, 59] by stretched Mittag–Leffler functions.

3. Anomalous diffusion by non-equilibrium statistical mechanics

3.1. Generalized Langevin equation

One of the most important steps in the theory of liquids was the introduction of the Generalized Langevin equation (GLE) by Zwanzig [5],

$$\dot{\boldsymbol{v}}(t) = -\int_0^t dt'\, \kappa\left(t-t'\right) \boldsymbol{v}\left(t'\right) + \boldsymbol{f}^{(+)}(t)\,. \tag{49}$$

The GLE describes the dynamics of a diffusing tagged particle in a many-body environment (typically a liquid) and can be considered as a "projected" equation of motion in which the environment of the diffusing particle is represented by the memory kernel and the fluctuating force $\boldsymbol{f}^{(+)}(t)$. The latter is not a stochastic force, as in Langevin's equation of motion for a Brownian particle [60] and corresponding generalized stochastic equations of motion [61, 62], but it can be formally constructed on the basis of the exact Hamiltonian dynamics of the total system, which comprises the tagged particle and its environment. The memory function is given by $\kappa(t) = \langle \boldsymbol{f}^{(+)}(0) \cdot \boldsymbol{f}^{(+)}(t)\rangle$, assuming an isotropic system. The details are not important here and can be found in the excellent book by Zwanzig on non-equilibrium statistical physics [6]. Using that, by construction, $\langle \boldsymbol{v}(0) \cdot \boldsymbol{f}^{(+)}(t)\rangle = 0$, one can derive a closed equation of motion for the velocity autocorrelation function (VACF),

$$\partial_t c_{vv}(t) = -\int_0^t dt'\, c_{vv}\left(t-t'\right) \kappa\left(t'\right)\,, \tag{50}$$

where the VACF is defined through the ensemble average,

$$c_{vv}(t) = \langle \boldsymbol{v}(t) \cdot \boldsymbol{v}(0)\rangle\,. \tag{51}$$

The memory function equation (50) has been the starting point for the development of numerous models for the dynamics of liquids [63, 64] and it proves also useful to understand the mechanisms of anomalous diffusion.

3.2. Asymptotic analysis of the diffusion regime

Any stochastic model for normal or anomalous diffusion implies an elimination of fast motions which are represented by noise and for this reason stochastic models can obviously not be applied on all time scales. Their applicability depends on the coarse-graining of the underlying time scale. If diffusion is modeled in position space, the MSD will, for example, not exhibit

the characteristic ballistic behavior $W(t) \sim \langle |\boldsymbol{v}|^2 \rangle \, t^2$ for short times, which follows from the Taylor expansion of expression (43). A rigorous analysis of diffusion processes can be accomplished within the framework of non-equilibrium statistical mechanics, which is based on deterministic equations of motion for the constituents of a many-body system. In this context, only the asymptotic form of the MSD is needed, since only this regime is relevant for diffusion processes. This section resumes the essential steps and results of two recent articles [65, 66] in which asymptotic analysis is used to establish the generalized Kubo formulae for transport coefficients, conditions for anomalous diffusion, and the applicability of fractional Fokker–Planck equations.

3.2.1. A Tauberian theorem for the mean square displacement

Referring to [65], a relation between the asymptotic regimes of the MSD and the VACF can be established through a theorem from asymptotic analysis, which falls into the category of Tauberian theorems. The Hardy–Littlewood–Karamata (HLK) theorem [67] yields a relation between the asymptotic form of functions $h(t)$ for which the integral $\int_0^\infty dt\, h(t)$ diverges and their Laplace transforms for small arguments s,

$$h(t) \overset{t\to\infty}{\sim} L(t) t^\rho \Leftrightarrow \hat{h}(s) \overset{s\to 0}{\sim} L(1/s) \frac{\Gamma(\rho+1)}{s^{\rho+1}}, \qquad \rho > -1\,. \tag{52}$$

Here, $L(t)$ is a "slowly growing function", fulfilling $\lim_{t\to\infty} L(\lambda t)/L(t) = 1$ for any $\lambda > 0$, and $\hat{h}(s) = \int_0^\infty dt\, \exp(-st) h(t)$ $(\Re\{s\} > 0)$ denotes the Laplace transform of $h(t)$. In the following, $L(t)$ fulfills the stronger conditions $\lim_{t\to\infty} L(t) = 1$ and $\lim_{t\to\infty} t\, dL(t)/dt = 0$. Theorem (52) may be applied to relate the asymptotic form of the MSD for long times to the asymptotic form of its Laplace transform for small s (compared to Ref. [65], where $W(t) \overset{t\to\infty}{\sim} 2D_\alpha t^\alpha$, D_α is here defined according to relation (14)),

$$W(t) \overset{t\to\infty}{\sim} \frac{2nD_\alpha}{\Gamma(1+\alpha)} L(t) t^\alpha \Leftrightarrow \hat{W}(s) \overset{s\to 0}{\sim} 2nD_\alpha L(1/s) \frac{1}{s^{\alpha+1}}\,. \tag{53}$$

Here, one may set $L(t) = 1$, but the possibility to make more sophisticated choices for $L(t)$ is explicitly maintained at this point. The very useful Laplace transform technique permits to express (43) in the form

$$\hat{W}(s) = \frac{2\,\hat{c}_{vv}(s)}{s^2} \tag{54}$$

and it follows from the memory function equation (50) that

$$\hat{c}_{vv}(s) = \frac{\langle |\boldsymbol{v}|^2 \rangle}{s + \hat{\kappa}(s)}\,, \tag{55}$$

noting that $\langle |\boldsymbol{v}|^2 \rangle = c_{vv}(0)$.

3.2.2. Generalized Kubo formula for D_α

Comparing (53) and (54) provides us with the asymptotic form for the Laplace-transformed VACF for small values of s,

$$\hat{c}_{vv}(s) \overset{s\to 0}{\sim} nD_\alpha L(1/s)s^{1-\alpha} \tag{56}$$

and this relation may be solved for D_α to give

$$D_\alpha = \lim_{s\to 0} \frac{s^{\alpha-1}\hat{c}_{vv}(s)}{n}\,. \tag{57}$$

Knowing that $s^{\alpha-1}\hat{c}_{vv}(s)$ is the Laplace transform of a fractional derivative of the order of $\alpha-1$ and that $\hat{f}(0) = \int_0^\infty dt\, f(t)$ for an arbitrary function f, it follows that

$$D_\alpha = \frac{1}{n}\int_0^\infty dt\, \partial_t^{\alpha-1} c_{vv}(t)\,, \qquad 0 \le \alpha < 2\,, \tag{58}$$

where the explicit form of the fractional derivative is

$$\partial_t^{\alpha-1} c_{vv}(t) = \frac{d}{dt}\int_0^t dt\, \frac{(t-\tau)^{1-\alpha}}{\Gamma(2-\alpha)} c_{vv}(\tau)\,. \tag{59}$$

For $\alpha = 1$, the standard Kubo formula,

$$D = \frac{1}{n}\int_0^\infty dt\, c_{vv}(t)\,, \tag{60}$$

is retrieved, but there is an important difference in the derivation. Kubo's derivation of transport coefficients [7] is based on linear response theory, whereas (58) relies on purely mathematical arguments.

3.2.3. Generalized Fluctuation-Dissipation Theorem

Combining relations (53), (54) and (55) leads to a direct relation between the Laplace-transformed MSD and the memory function of the VACF for small values of s,

$$\hat{W}(s) \overset{s\to 0}{\sim} \frac{\langle |\boldsymbol{v}|^2 \rangle}{s^2\hat{\kappa}(s)}\,. \tag{61}$$

Here, the assumption $s^3 \ll s^2\hat{\kappa}(s)$ has been made, which is correct for $s \to 0$ if ballistic diffusion is excluded. Equating expressions (53) and (61) leads then to the asymptotic form of the memory kernel for small values of s,

$$\hat{\kappa}(s) \overset{s\to 0}{\sim} \frac{\langle|\boldsymbol{v}|^2\rangle}{nD_\alpha}\frac{s^{\alpha-1}}{L(1/s)}\,. \tag{62}$$

Similarly to the fractional diffusion coefficient, one can define a fractional relaxation constant through

$$\eta_\alpha = \lim_{s\to 0} s^{1-\alpha}\hat{\kappa}(s)\,. \tag{63}$$

In the time domain, this relation reads

$$\eta_\alpha = \int_0^\infty dt\, \partial_t^{1-\alpha}\kappa(t)\,, \tag{64}$$

where (see Eq. (5))

$$\partial_t^{1-\alpha}\kappa(t) = \frac{d}{dt}\int_0^t d\tau\, \frac{(t-\tau)^{\alpha-1}}{\Gamma(\alpha)}\kappa(t)\,.$$

It should be noted that the order of the derivative is here $1-\alpha$, whereas it is $\alpha - 1$ in the case of the fractional diffusion constant (58).

Expressions (58) and (64) may be connected in form of a generalized Fluctuation-Dissipation Theorem,

$$D_\alpha = \frac{\langle|\boldsymbol{v}|^2\rangle}{n\,\eta_\alpha}\,. \tag{65}$$

3.2.4. Long-time tails for the VACF and its memory function

A closer look at expressions (56) and (62) shows that $\hat{c}_{vv}(s)/s \propto s^{-\alpha}$ and that $\hat{\kappa}(s)/s \propto s^{\alpha-2}$. Both $s^{-\alpha}$ and $s^{\alpha-2}$ diverge if $0 \le \alpha < 2$ and knowing that the Laplace transform of an integral of the form $\int_0^t d\tau\, f(\tau)$ is $\hat{f}(s)/s$, it follows from the HLK theorem that

$$f(t) = \int_0^t d\tau c_{vv}(\tau) \overset{t\to\infty}{\sim} \frac{nD_\alpha L(t)}{\Gamma(\alpha)}t^{\alpha-1}\,, \tag{66}$$

$$g(t) = \int_0^t d\tau\kappa(\tau) \overset{t\to\infty}{\sim} \frac{\langle|\boldsymbol{v}|^2\rangle}{D_\alpha n\Gamma(2-\alpha)L(t)}t^{1-\alpha}\,. \tag{67}$$

Here, it has been used that if $L(t)$ is a slowly growing function, the same is true for $1/L(t)$. Differentiating $f(t)$ and $g(t)$ yields then *necessary* conditions for the long-time tails of the VACF and its memory function

$$c_{vv}(t) \overset{t\to\infty}{\sim} \frac{nD_\alpha L(t) t^{\alpha-2}}{\Gamma(\alpha-1)}\,, \tag{68}$$

$$\kappa(t) \overset{t\to\infty}{\sim} \frac{\langle |\boldsymbol{v}|^2 \rangle\, t^{-\alpha}}{\Gamma(1-\alpha) n D_\alpha L(t)}\,. \tag{69}$$

The HLK theorem shows that these conditions are also *sufficient* for the VACF if $1 < \alpha < 2$ (superdiffusion) and for the corresponding memory functions if $0 \leq \alpha < 1$. This means that subdiffusion is equivalent with the asymptotic form (68) of the memory function and that superdiffusion is equivalent with the asymptotic form (69) of the VACF.

Figure 6 displays the α-dependent weights of the long-time tails. One recognizes that the VACF has a negative long-time tail for subdiffusion ($0 < \alpha < 1$) and a positive long-time tail for superdiffusion ($1 < \alpha < 2$). This can be understood as follows. In the case of subdiffusion, anticorrelations between the velocities at times τ and $\tau + t$, respectively, persist for long lag times t, indicating that the diffusing particle tends to invert its velocity to go back to the point of departure. Negative velocity correlations, in general, are referred to as "cage effect" in the theory of liquids, and subdiffusion indicates a persisting cage. In the case of superdiffusion, one finds exactly the opposite. Here, positive autocorrelations between velocities for two different lag times persist and reflect a sort of "anti-cage", namely that the diffusing particle is essentially repelled from its local environment, which leads to accelerated diffusion. It should be noted that the signs of the long-time tails for the VACF and its memory function are opposite and that they vanish for $\alpha = 1$, *i.e.* in the case of normal diffusion.

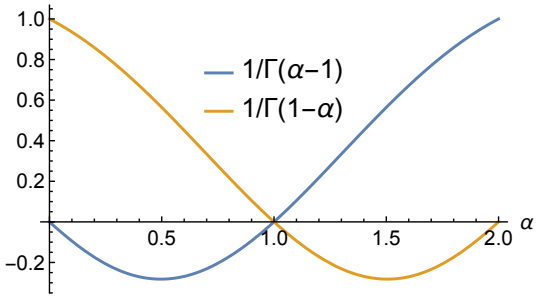

Fig. 6. α-dependence of the long-time tails of the VACF (black/blue) and its memory function (light gray/dark yellow).

3.3. Anomalous Brownian motion and time scale separation

In Section 2.5, it has been reported that a particle whose velocity follows a fractional Ornstein–Uhlenbeck process in velocity space exhibits anomalous free diffusion in position space [36]. According to Eq. (41), the corresponding VACF has the form of a "stretched" Mittag–Leffler function. The anomaly of the diffusion process is steered by the parameter ρ, which varies between 0 and 2. For $\rho = 1$, normal diffusion is retrieved and the VACF becomes an exponential function. Since the first computer simulation of simple liquids [27], it has been known that the VACF of a molecule is not an exponential function, but exhibits a regime of negative values. This reflects a caging effect through the neighboring molecules which make the diffusing particle invert its direction. An exponentially relaxing VACF indicates a time scale separation between the slowly diffusing tagged particle and the fast motions of the surrounding liquid molecules. Such a time scale separation is characteristic for Brownian motion, where one considers the diffusion of a heavy particle in a bath of light particles. Molecular dynamics simulations are a beautiful tool to investigate the effect of time scale separation empirically, increasing gradually the mass of the diffusing particle with respect to the mass of the solvent molecules [68]. When the mass of a selected tracer particle is increased, one sees, indeed, that its VACF takes a more and more exponential form and varies at the same time more and more slowly. In Ref. [69], it has been shown that this can be understood on the basis of a scaling of the memory function, which scales inverse proportional to the (reduced) mass of the diffusing particle,

$$\kappa(t) \;\rightarrow\; \lambda\kappa(t)\,, \tag{70}$$

$$m \;\rightarrow\; m/\lambda\,, \tag{71}$$

where $\lambda \to 0$. In a recent article [66], I have shown that the same scaling procedure leads to VACFs of the form (41) if the starting point is a simple liquid in which all molecules perform anomalous free diffusion. The details of this somewhat more tricky scaling approach can be found in [66]. As a result of the scaling process (70)/(71) the VACF approaches

$$\psi_\lambda(t) \approx E_{2-\alpha}\left(-\left[t/\tau_v^{(\lambda)}\right]^{2-\alpha}\right)\,, \tag{72}$$

where $\tau_v^{(\lambda)}$ is the time scale of the "slow" tracer particles

$$\tau_v^{(\lambda)} = \frac{\tau_v}{\lambda^{1/(2-\alpha)}} \gg \tau_v \tag{73}$$

with τ_v being the velocity time scale of the "fast" solvent molecules. Using the definition (14) to define the fractional diffusion constant, the velocity

time scale is set through

$$\tau_v = \left(\frac{n D_\alpha}{\langle |\boldsymbol{v}|^2 \rangle} \right)^{1/(2-\alpha)} . \tag{74}$$

Figure 7 shows the result of the scaling procedure for a numerical example, in which the memory function has the form

$$\kappa(t) = \Omega^2 M\left(\alpha, 1, -t/\tau_{\mathrm{m}}\right) . \tag{75}$$

Here, $M(a, b, z)$ is Kummer's hypergeometric function [16], $\kappa(0) = \Omega^2$, and Ω has the dimension of a frequency. The parameter τ_{m} sets the time scale of the memory function. Since the Laplace transform of the memory function behaves for small s as $s^{\alpha-1}$, condition (62) is verified. The corresponding diffusion constant is found to be

$$D_\alpha = \frac{\left\langle |\boldsymbol{v}|^2 \right\rangle \tau_{\mathrm{m}}^{-\alpha}}{n\, \Omega^2} \tag{76}$$

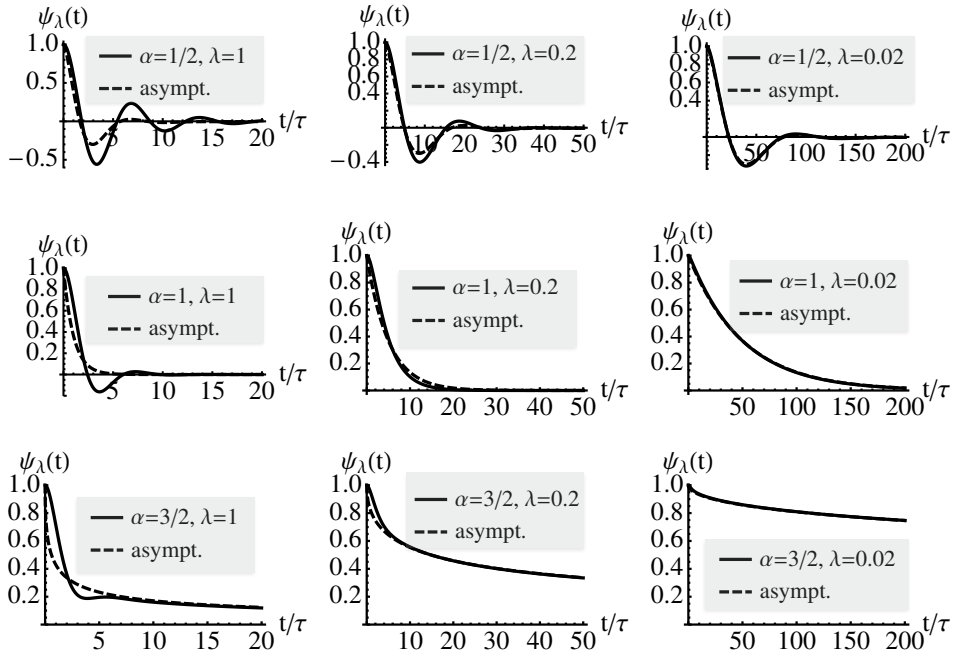

Fig. 7. Velocity autocorrelation functions $\psi_\lambda(t)$ for different scaling factors λ (solid lines) and corresponding asymptotic approximations (72) (dashed lines). From top to bottom $\alpha = 1/2,\ 1,\ 3/2$, from left to right $\lambda = 1,\ 0.2,\ 0.02$. The amplitude of the memory function is chosen as $\Omega = 1/\tau_{\mathrm{m}}$, such that $\tau = \tau_{\mathrm{m}}$.

and the characteristic velocity time reads

$$\tau_v = \left(\frac{\tau_{\mathrm{m}}^{-\alpha}}{\Omega^2} \right)^{\frac{1}{2-\alpha}} . \tag{77}$$

It is clearly visible that the exact VACFs (solid lines) tend rapidly to the limiting forms (72) (dashed lines) as λ tends to zero. Here, it must be emphasized that a strict limit $\lambda \to 0$ cannot be performed since the VACF would not change at all. This short paragraph has thus shown that the VACF of the anomalous Rayleigh particle corresponds to the Brownian limit, in which the mass of the diffusing particle is much bigger than the mass of the solvent molecules. It is thus the natural generalization of the exponentially decaying VACF of the Rayleigh particle, which is retrieved for $\alpha = 1$.

3.4. Confined anomalous diffusion

3.4.1. Memory kernel and anomalous relaxation

Spatially confined diffusion, where the motions of the diffusing particle are confined by a container of finite size or by external forces, merits a separate discussion. Here, $\alpha = 0$, which expresses that the MSD tends to a plateau value for long times,

$$W(t) \overset{t\to\infty}{\sim} 2nD_0 L(t) . \tag{78}$$

As discussed earlier, one considers effectively the MSD of $\boldsymbol{u}(t) = \boldsymbol{r}(t) - \langle \boldsymbol{r} \rangle$ in this case and the corresponding fractional diffusion coefficient D_0 can be formally obtained from the generalized Kubo relation (58)

$$D_0 = \frac{1}{n} \left\langle |\boldsymbol{u}|^2 \right\rangle . \tag{79}$$

This is in agreement with the general physical dimension of D_α, which is length^2/time$^\alpha$. It follows from expression (68) that the memory function has the general asymptotic form

$$\kappa(t) \overset{t\to\infty}{\sim} \frac{\left\langle |\boldsymbol{v}|^2 \right\rangle}{\left\langle |\boldsymbol{u}|^2 \right\rangle} \frac{1}{L(t)} . \tag{80}$$

This expression can be understood by setting $L(t) = 1$. In this case, the asymptotic form of the memory function is a constant, $\kappa(t) \overset{t\to\infty}{\sim} \Omega^2$, where Ω is defined through $\Omega = \sqrt{\langle |\boldsymbol{v}|^2 \rangle / \langle |\boldsymbol{u}|^2 \rangle}$. The resulting asymptotic VACF is simply a cosine function, $c_{vv}(t) = \langle |\boldsymbol{v}|^2 \rangle \cos(\Omega t)$, describing a "rattling" motion of the diffusing particle in the cage represented by its environment.

This is, of course, to some extent an unphysical picture since the rattling motion is undamped and one expects damping effects by collisions with the neighbors. A more refined description of the diffusion process is, in fact, obtained by taking into account the function $L(t)$, and normal and anomalous diffusion must be distinguished on the basis of the asymptotic form of $L(t)$. Following [65], confined diffusion is said to be anomalous if the relaxation time

$$\tau_c = \int_0^\infty dt\, \frac{\kappa(t) - \kappa(\infty)}{\kappa(0) - \kappa(\infty)} \tag{81}$$

diverges. This is the case if

$$\frac{1}{L(t)} - 1 \overset{t\to\infty}{\sim} C\, t^{-\beta} \qquad \text{and} \qquad 0 < \beta \leq 1\,, \tag{82}$$

where $C > 0$ is a constant. Relation (82) is obtained if $L(t)$ has the form $L(t) \overset{t\to\infty}{\sim} 1 - Ct^{-\beta}$ and with (15) this corresponds to saying that the DACF decays anomalously slowly,

$$\frac{c_{uu}(t)}{c_{uu}(0)} \overset{t\to\infty}{\sim} Ct^{-\beta}\,. \tag{83}$$

The above considerations show that anomalous relaxation in position space is a direct consequence of the slow power law approach of the memory kernel to its plateau value. Using the cage picture for the environment of the diffusing particle, relation (82) reflects a slowly decaying cage towards its plateau value. The persistence of the cage for arbitrarily long times prevents the diffusing particle from escaping to infinity.

3.4.2. Relaxation rate spectra

The relaxation rate spectrum of a slowly decaying DACF has a particular form, which can be used to build relaxation models. Referring to Section 2.4.3, the relaxation function $\psi(t) = c_{uu}(t)/c_{uu}(0)$ is represented in the form

$$\psi(t) = \int_0^\infty d\lambda\, p(\lambda) \exp(-\lambda t)\,,$$

and the relation between the relaxation function and its relaxation spectrum is given by the Stieljes transform pair

$$\begin{aligned}\hat{\psi}(s) &= \int_0^\infty d\lambda\, \frac{p(\lambda)}{s+\lambda}\,,\\ p(\lambda) &= \frac{1}{\pi}\lim_{\epsilon\to 0}\Im\left\{\hat{\psi}(-\lambda - i\epsilon)\right\}\,.\end{aligned}$$

In the case of anomalous relaxation, where the DACF decays asymptotically as in (83), it follows from the HLK-theorem (52) that

$$\psi(t) \overset{t\to\infty}{\sim} t^{-\beta} \Leftrightarrow \hat{\psi}(s) \overset{s\to 0}{\sim} \frac{\Gamma(1-\beta)}{s^{1-\beta}}\,, \tag{84}$$

and, therefore, $p(\lambda)$ must have the general form [70]

$$p(\lambda) = f(\lambda)\frac{\sin(\pi\beta)}{\pi}\frac{\Gamma(1-\beta)}{\lambda^{1-\beta}}\,, \qquad 0<\beta\le 1\,. \tag{85}$$

The function $f(\lambda)$ is yet undetermined and must be chosen such that $\lim_{\lambda\to 0} f(\lambda) = \text{const}$ and that $\int_0^\infty p(\lambda;\beta) = 1$. The special choice [70]

$$f(\lambda) = \exp(-\beta\lambda) \tag{86}$$

ensures that all moments of the relaxation spectra exist, which are defined through

$$\overline{\lambda^k} = \int_0^\infty d\lambda\, \lambda^k p(\lambda) = (-1)^k \psi^{(k)}(0)\,. \tag{87}$$

The correctly normalized relaxation rate spectrum for corresponding to the choice (86) is

$$p(\lambda;\beta) = \frac{\lambda^{\beta-1}\beta^\beta \exp(-\beta\lambda)}{\Gamma(\beta)}\,, \tag{88}$$

and the corresponding relaxation function $\psi(t)$ reads

$$\psi(t;\beta) = \frac{1}{(1+t/\beta)^\beta}\,. \tag{89}$$

It is worthwhile noting that $\psi(t;\beta)$ yields the Tsallis exponential function by setting $\beta = 1/(1-q)$ [71–73]. One realizes that

$$\lim_{\beta\to\infty}\psi(t;\beta) = \exp(-t) \tag{90}$$

and, therefore,

$$\lim_{\beta\to\infty} p(\lambda;\beta) = \delta(\lambda - 1)\,. \tag{91}$$

The cumulants of $p(\lambda;\beta)$, which are defined through

$$c_\beta^{(k)} = (-1)^k \left.\frac{d^k}{dt^k} \ln(\psi(t;\beta))\right|_{t=0+}\,, \tag{92}$$

have a particularly simple form

$$c_{\alpha,\beta}^{(1)} = 1\,, \tag{93}$$

$$c_{\alpha,\beta}^{(k)} = \frac{(k-1)!}{\beta^{k-1}}\,, \qquad k = 2, 3, \ldots \tag{94}$$

Figure 8 displays the relaxation function (97) for several values of β and the corresponding relaxation rate spectra. These curves should be compared to their counterparts for the fOU process, which have been presented in Fig. 1. The initial decay of the relaxation function in the latter case is visibly steeper. It follows, in fact, from (35) that all derivatives of $\psi_{\mathrm{fOU}}(t;\beta)$ diverge at $t = 0$, $(-1)^k \psi_{\mathrm{fOU}}^{(k)}(0;\beta) = +\infty$. Therefore, all moments $\overline{\lambda^k}$ diverge for $k \geq 1$ according to relation (87).

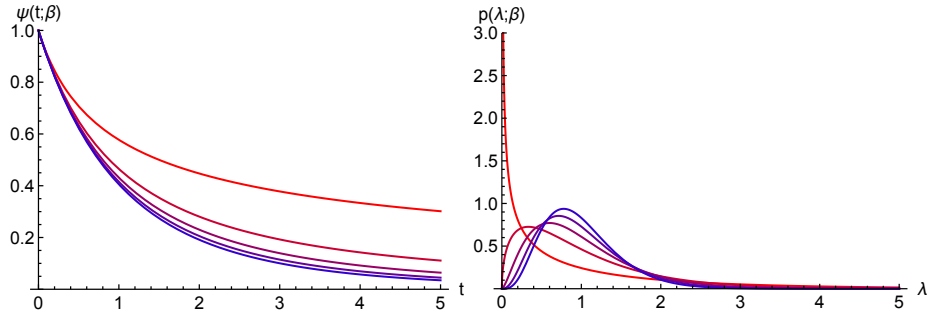

Fig. 8. Left: Normalized DACF $\psi(t;\beta)$ for $\beta = 0.5, 1.5, \ldots, 4.5$ (curves from top to bottom/red to blue on-line) Right: Corresponding relaxation spectra $p(\lambda;\beta)$.

3.5. Illustrations

3.5.1. VACF for lateral motions of lipid molecules

In the following, we go briefly back to Section 2.6.1, in which two examples for subdiffusion in lipid bilayers have been given. A more detailed analysis of the VACF describing the lateral center-of-mass motion of the

DOPC lipids illustrates expressions (69) and (68) for, respectively, the long-time tail of the VACF and its memory function. The left part of Fig. 9 shows first of all that the VACF of a lipid molecule has a negative long time tail and the inset shows that the theoretical form (69) superposes well with the simulated VACF for $t > 1$ ps. We note here that, according to (74), the relaxation time of the VACF is

$$\tau_v \approx 0.23\,\text{ps} \tag{95}$$

if the definition (14) for D_α is used. The concrete value of τ gives an indication of what "asymptotically" means in practice and one sees that the asymptotic regime starts already in the picosecond range. The right part of Fig. 9 displays the simulated memory function, where the inset shows, again, the theoretical longtime tail superposed to the simulated function. The decay of the memory function is extremely steep, of the order of a few integration time steps, and the dynamics is probably not well enough resolved for a detailed analysis. The figure shows, however, clearly a qualitative agreement between the simulated function and the theoretical long-time tail (68). It should, in particular, be noted that the simulated long-time tails of the VACF and its memory function have opposite signs, as required by the theoretical considerations for the case of subdiffusion.

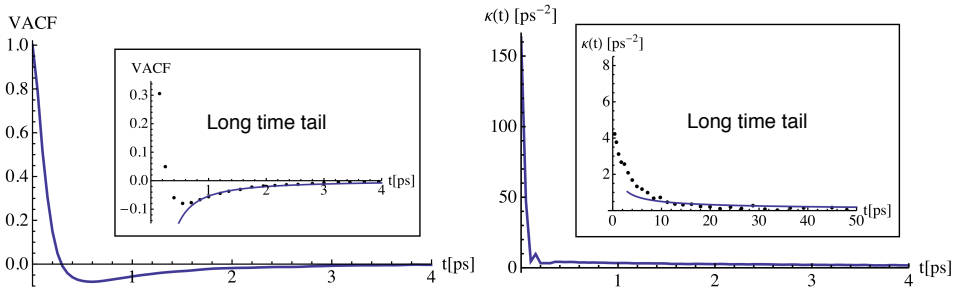

Fig. 9. Left: Normalized VACF for the lateral CM motion of the DOPC molecules. The inset shows the simulated VACF (dots) together with the long-time tail (69) with $L(t) = 1$ (solid line). Right: The corresponding memory function. The inset shows the superposition of the simulated memory function (dots) with the corresponding long-time tail (68) with $L(t) = 1$ (solid line).

3.5.2. Backbone relaxation in proteins

This section is devoted to the presentation of a model for the relaxation and diffusion dynamics for the main chain of proteins, which has been recently published [70]. The idea was to test a model based on the theoretical considerations presented in Section 3.4.2, which would, in particular, lead to

finite moments of the relaxation rate spectrum and, therefore, to displacement autocorrelation functions which are differentiable at $t = 0$. As already mentioned, this is not the case if the underlying dynamical model is an fOU process. The dynamical model to be briefly discussed in the following is a coarse-grained model in which a protein is represented only by the so-called C_α-atoms along the protein main chain, which are the anchor points of the side chains. Writing the displacement autocorrelation for the C_α-atoms as

$$c_{uu}(t) = \langle |\boldsymbol{u}|^2 \rangle \, \psi(t) \,, \tag{96}$$

the relaxation function for the model reads

$$\psi(t; \alpha; \beta) = \frac{\exp(-\alpha t)}{(1 + t/\beta)^\beta} \,. \tag{97}$$

The corresponding relaxation spectrum has the form

$$p(\lambda; \beta; \alpha) = p_0(\lambda - \alpha; \beta; \alpha) \,, \tag{98}$$

where $p_0(\lambda; \beta; \alpha)$ is given by expression (88),

$$p_0(\lambda; \beta) = \frac{\lambda^{\beta-1} \beta^\beta \exp(-\beta\lambda)}{\Gamma(\beta)} \,. \tag{99}$$

The model relaxation spectrum (98) is thus a shifted form of $p_0(\lambda; \beta)$, with a cut-off at $\lambda = \alpha$ at the lower end of the relaxation rate spectrum. Only for $\alpha = 0$ and $0 < \beta < 1$, the relaxation is anomalous. The corresponding cumulants of the relaxation rate spectrum are the same as for $p_0(\lambda; \beta)$, except the first one

$$c^{(1)}_{\alpha,\beta} = 1 + \alpha \,, \tag{100}$$

$$c^{(k)}_{\alpha,\beta} = \frac{(k-1)!}{\beta^{k-1}} \,, \qquad k = 2, 3, \ldots \tag{101}$$

A coherent view of the results for a concrete time scale τ is obtained by looking at

— the mean relaxation rate, $\overline{\lambda} = (1 + \alpha)\tau^{-1}$,

— the corresponding spread, $\sigma_\lambda = \left(\overline{\lambda^2} - \overline{\lambda}^2\right)^{1/2} = \beta^{-1/2}\tau^{-1}$,

— the mean square position fluctuation $\langle |\boldsymbol{u}|^2 \rangle$,

— the short time diffusion coefficient, $D_\mathrm{s} = \langle |\boldsymbol{u}|^2 \rangle \overline{\lambda}$,

and to correlate the results with the solvent accessible surface (SAS). The results are given in Fig. 10, where the sketch on top of the figure indicates secondary structure elements. These are α-helices (black rectangles), short helicoidal motifs (grey rectangles) and β-strands (arrows). The vertical dotted lines locate four selected residues, two of which are in α-helices (Ala 9 and Val 29) and two in loops (Thr 47 and Gly 104). These residues are also indicated in Fig. 11. The results show that fast relaxation is strongly correlated with a broad relaxation spectrum, which applies, in particular, to residues with a low SAS. This effect is particularly pronounced for the "buried" residues Ala 9 and Val 29. The fast relaxation of buried residues

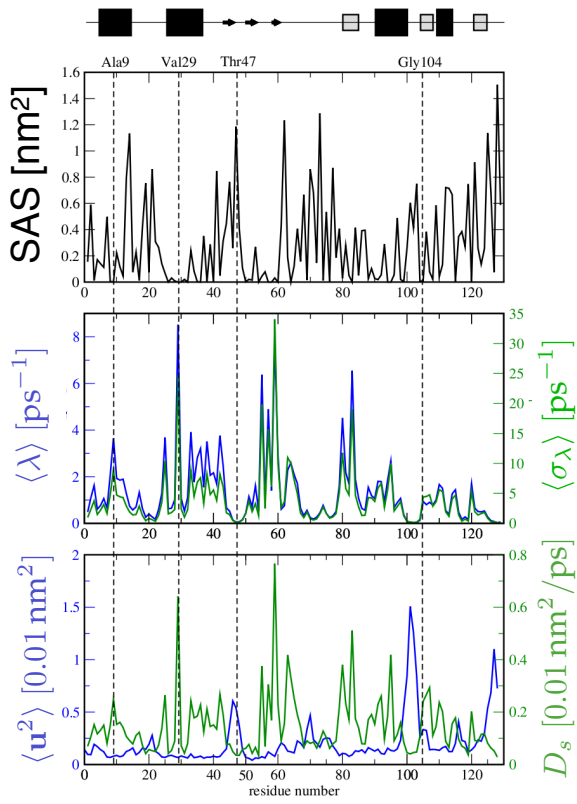

Fig. 10. Upper panel: Solvent accessible surface for the C_α-atoms in lysozyme. Middle panel: Mean relaxation rate $\overline{\lambda}$ (blue/dark gray line) and corresponding standard deviation σ_λ (green/light gray line). Lower panel: Mean square position fluctuation $\langle|\boldsymbol{u}|^2\rangle$ (blue/dark gray line) and short time diffusion coefficient D_s (green/light green line). The graphics on top indicate secondary structure elements, where black rectangles stand for α-helices, gray, rectangles short helicoidal motifs and arrows, beta strands.

can be understood by the picture of frequent collisions with adjacent atoms and the large spread of relaxation rates reflects strong correlations between their motions and those of the atoms in the environment. The lower part of Fig. 11 shows that large position fluctuations are seen in loop regions, but more surprisingly, that the short time diffusion coefficients are the highest for residues with small SAS, although the position fluctuations in these regions are small. The $\overline{\lambda}$-factor in the short time diffusion coefficient is thus dominant.

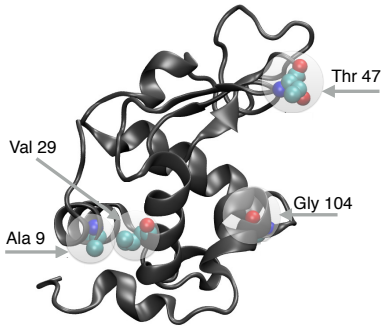

Fig. 11. Protein main chain of lysozyme and four selected residues.

4. Conclusions

The idea of this short review was to present models for anomalous diffusion in complex biomolecular systems in the framework of non-equilibrium statistical physics, which is the theoretical basis to understand the structure and dynamics of liquids. In this context, a Tauberian theorem from asymptotic analysis was an essential element to generalize the well-known Kubo expressions for diffusion-related transport coefficients to the case of anomalous diffusion. It was also shown that general conditions for anomalous diffusion can be derived by applying asymptotic analysis to the generalized Langevin equation and that this approach yields well-defined characteristic time scales as well as insight into the validity of diffusion models. The approach may, moreover, be used to construct physically meaningful relaxation and diffusion models for protein dynamics. In order to illustrate the theoretical concepts, several applications were presented for simulation studies of protein dynamics and anomalous diffusion of molecules in lipid bilayers. It has been in particular demonstrated that molecular dynamics simulation is an invaluable tool to gain insight into transport and relaxation processes in "crowded" biomolecular systems.

REFERENCES

[1] B.B. Mandelbrot, J.W. Van Ness, *SIAM Rev.* **10**, 422 (1968).

[2] H. Scher, E.W. Montroll, *Phys. Rev. B* **12**, 2455 (1975).

[3] R. Metzler, J. Klafter, *Phys. Rep.* **339**, 1 (2000).

[4] I.M. Sokolov, *Soft Matter* **2012(8)**, 9043 (2012).

[5] R. Zwanzig, Statistical Mechanics of Irreversibility, *Lectures in Theoretical Physics*, Wiley-Interscience, New York 1961, pp. 106–141.

[6] R. Zwanzig, *Nonequilibrium Statistical Mechanics*, Oxford University Press, 2001.

[7] R. Kubo, *J. Phys. Soc. Jpn.* **12**, 570 (1957).

[8] A. Fick, *Ann. d. Physik* **170**, 59 (1855).

[9] H. Freundlich, D. Krüger, *Trans. Faraday Soc.* **31**, 906 (1935).

[10] P. Schwille, J. Korlach, W. Webb, *Cytometry* **36**, 176 (1999).

[11] T.V. Ratto, M.L. Longo, *Langmuir* **19**, 1788 (2003).

[12] K. Dworecki, *Physica A* **359**, 24 (2006).

[13] W. Wyss, *J. Math. Phys.* **27**, 2782 (1986).

[14] K.B. Oldham, J. Spanier, *The Fractional Calculus*, Academic Press, New York, London 1974.

[15] S.G. Samko, A.A. Kilbas, O.I. Marichev, *Fractional Integrals and Derivatives*, Gordon and Breach Science Publishers, 1993.

[16] F.W.J. Olver, D.W. Lozier, R.F. Boisvert, Ch.W. Clark (Eds.), *NIST Handbook of Mathematical Functions*, Cambridge University Press, 2010.

[17] A. Einstein, *Ann. d. Physik* **322**, 549 (1905).

[18] M. von Smoluchowski, Essai d'une théorie cinétique du mouvement brownien et des milieux troublés, *Bulletin International de l'Académie des Sciences de Cracovie*, pp. 577–602, 1906.

[19] M. von Smoluchowski, Sur le chemin moyen parcouru par les molécules d'un gaz et sur son rapport avec la théorie de la diffusion, *Bulletin International de l'Académie des Sciences de Cracovie*, pp. 202–213, 1906.

[20] M. von Smoluchowski, *Ann. d. Physik* **326**, 756 (1906).

[21] C.W. Gardiner, *Handbook of Stochastic Methods*, Springer Series in Synergetics, Springer, Berlin–Heidelberg–New York 1985, 2$^{\text{nd}}$ edition.

[22] A. Papoulis, *Probablity, Random Variables, and Stochastic Processes*, McGraw Hill, New York 1991, 3$^{\text{rd}}$ edition.

[23] N.G. van Kampen, *Stochastic Processes in Physics and Chemistry*, North Holland, Amsterdam 1992, revised edition.

[24] B.M. Regner *et al.*, *Biophys. J.* **104**, 1652 (2013).

[25] S. Burov, J.-H. Jeon, R. Metzler, E. Barkai, *Phys. Chem. Chem. Phys.* **13**, 1800 (2011).

[26] A. Lubelski, I. Sokolov, J. Klafter, *Phys. Rev. Lett.* **100**, 250602 (2008).

[27] A. Rahman, *Phys. Rev.* **136**, 405 (1964).
[28] M.P. Allen, D.J. Tildesley, *Computer Simulation of Liquids*, Oxford University Press, Oxford 1987.
[29] H. Risken, *The Fokker–Planck Equation*, Springer Series in Synergetics, Springer, Berlin–Heidelberg–New York 1996, 2nd reprinted edition.
[30] M. von Smoluchowski, *Ann. d. Physik* **353**, 1103 (1916).
[31] F. Matthäus, M. Jagodič, J. Dobnikar, *Biophys. J.* **97**, 946 (2009).
[32] Y. Shao, *Physica D: Nonlinear Phenomena* **83**, 461 (1995).
[33] G.R. Kneller, *Phys. Chem. Chem. Phys.* **7**, 2641 (2005).
[34] W.G. Glöckle, T.F. Nonnenmacher, *Biophys. J.* **68**, 46 (1995).
[35] A. Erdélyi, W. Magnus, F. Oberhettinger, F.G. Tricomi, *Higher Transcendental Functions*, McGraw Hill, New York 1955.
[36] E. Barkai, R.J. Silbey, *J. Phys. Chem. B* **104**, 3866 (2000).
[37] G.R. Kneller, K. Baczynski, M. Pasenkiewicz-Gierula, *J. Chem. Phys.* **135**, 141105 (2011).
[38] E. Flenner, J. Das, M.C. Rheinstädter, I. Kosztin, *Phys. Rev.* **E79**, 11907 (2009).
[39] J.-H. Jeon, H.M.S. Monne, M. Javanainen, R. Metzler, *Phys. Rev. Lett.* **109**, 188103 (2012).
[40] S. Stachura, G.R. Kneller, *Mol. Simulat.* **40**, 245 (2014).
[41] W.L. Jorgensen, J. Tirado-Rives, *J. Am. Chem. Soc.* **110**, 1657 (1988).
[42] W.L. Jorgensen, D.S. Maxwell, J. Tirado-Rives, *J. Am. Chem. Soc.* **118**, 11225 (1996).
[43] S.J. Marrink, A.H. de Vries, A.E. Mark, *J. Phys. Chem. B* **108**, 750 (2004).
[44] S.J. Marrink *et al.*, *J. Phys. Chem. B* **111**, 7812 (2007).
[45] H. Frauenfelder, G.A. Petsko, D. Tsernoglou, *Nature* **280**, 558 (1979).
[46] H. Hartmann *et al.*, *Proc. Natl. Acad. Sci. USA* **79**, 4967 (1982).
[47] W. Doster, S. Cusack, W. Petry, *Nature* **337**, 754 (1989).
[48] G. Zaccai, *Science* **288**, 1604 (2000).
[49] R.H. Austin *et al.*, *Biochemistry* **14**, 5355 (1975).
[50] H. Frauenfelder, S.G. Sligar, P.G. Wolynes, *Science* **254**, 1598 (1991).
[51] H. Yang *et al.*, *Science* **302**, 262 (2003).
[52] W. Min *et al.*, *Phys. Rev. Lett.* **94**, 198302 (2005).
[53] V. Calandrini *et al.*, *Chem. Phys.* **345**, 289 (2008).
[54] V. Calandrini, D. Abergel, G.R. Kneller, *J. Chem. Phys.* **128**, 145102 (2008).
[55] V. Calandrini, D. Abergel, G.R. Kneller, *J. Chem. Phys.* **133**, 45101 (2010).
[56] P.A. Calligari, D. Abergel, *J. Phys. Chem. B* **116**, 12955 (2012).
[57] P. Calligari, V. Calandrini, G.R. Kneller, D. Abergel, *J. Phys. Chem. B* **115**, 12370 (2011).

[58] G. Lipari, A. Szabo, *J. Am. Chem. Soc.* **104**, 4546 (1982).
[59] G. Lipari, A. Szabo, *J. Am. Chem. Soc.* **104**, 4559 (1982).
[60] P. Langevin, *C. R. Acad. Sci. (Paris)* **146**, 530 (1908).
[61] E. Lutz, *Phys. Rev.* **E64**, 051106 (2001).
[62] S.C. Kou, X.S. Xie, *Phys. Rev. Lett.* **93**, 180603 (2004).
[63] J.P. Boon, S. Yip, *Molecular Hydrodynamics*, McGraw Hill, New York 1980.
[64] J.-P. Hansen, I.R. McDonald, *Theory of Simple Liquids*, Academic Press, 1986, 2nd edition.
[65] G.R. Kneller, *J. Chem. Phys.* **134**, 224106 (2011).
[66] G.R. Kneller, *J. Chem. Phys.* **141**, 041105 (2014).
[67] J. Karamata, *Journal für die reine und angewandte Mathematik (Crelle's Journal)* **1931**, 27 (1931).
[68] G.R. Kneller, K. Hinsen, G. Sutmann, *J. Chem. Phys.* **118**, 5283 (2003).
[69] G.R. Kneller, G. Sutmann, *J. Chem. Phys.* **120**, 1667 (2004).
[70] G.R. Kneller, K. Hinsen, P. Calligari, *J. Chem. Phys.* **136**, 191101 (2012).
[71] C. Tsallis, *J. Stat. Phys.* **52**, 479 (1988).
[72] M.L. Lyra, C. Tsallis, *Phys. Rev. Lett.* **80**, 53 (1998).
[73] J. Naudts, *J. Phys.: Conf. Series* **201**, 012003 (2010).